Kovove Mater. 60 2022 79–87
DOI: 10.31577/km.2022.2.79

Evolution of the AA2030 alloy microstructure in the ECAP process

Violetta A. Andreyachshenko*

Karaganda Technical University, Test Laboratory of Engineering Profile, Complex Development of Mineral Resources, Karaganda, Kazakhstan

Received 28 October 2020, received in revised form 11 February 2022, accepted 7 April 2022

Abstract

This work aims to study the microstructural development of lead-containing aluminum alloy in the process of intense plastic deformation. The evolution of the AA2030 alloy obtained by the ECAP and long-term natural aging (within 45 months) has been analyzed using electron microscopes. The average grain size of the ECAP treated samples is 420 and 380 nm along the routes B_c and C, respectively. Long-term natural aging contributes to transforming grain boundaries without changing their size. The results have shown that the structure, phase distribution, and stoichiometric composition of the inclusions differ significantly during annealing, equal-channel angular pressing, and long-term natural aging. The strain route affects the dissolution kinetics and evolution of inclusions. A mechanism for refining the grains is proposed that is associated with high dislocation density, dislocation cells, grain and subgrain boundaries, as well as the evolution of inclusions in the ECAP AA2030 alloys.

K e y w o r d s: aluminum alloys, AA2030, SPD, ECAP, grains and interfaces, electron microscopy

1. Introduction

In recent decades, research and development of bulk nanostructured materials or ultrafine-grained (UFG) materials obtained by severe plastic deformation (SPD) methods have received a huge breakthrough [1–5]. Earlier, we also performed several studies on evaluating the SPD effect on the microstructure and deformation behavior of steel and aluminum alloys [6–10]. It is known that AA2XXX series alloys are widely applicable in the automotive and aviation industries [11]. Effective hardening of alloys of this series is achieved by both thermal and deformation methods. In work [12], an increase in strength due to laser treatment was noted, but the hardening mechanism in this process is not clear. Alloys of this series belong to thermally hardened alloys, and dispersoids act as a hardening phase. The authors of [13] studied in detail the process of alloy hardening due to the formation of S inclusions – Al_2CuMg. In addition, dispersed particles of Mg_2Si and θ-Al_2Cu are also strengthening.

Despite such properties of AA2XXX series alloys as high strength and high ductility, for successful application in the industry, it is necessary to ensure the alloy also with good treatability, which is achieved by adding lead (free-cutting Al-alloys) [14, 15]. This is connected with the formation of low-melting Pb-enriched eutectics with low melting points. The impact of Pb-enriched inclusions provides ease of cutting. In addition, the impact of Pb also causes increasing wear resistance [16, 17]. To this end, lead is present in such alloys as AA6012, AA6262, AA2011, AA2030, and EN-AW 2007 [18, 19].

The AA2030 (Al-Cu-Pb-Mg-Mn-Si) alloy is of interest since it has been specially developed for the automotive industry; it belongs to thermally hardened alloys, while aging can be both artificial and natural. The effect of the aging process of the AA2030 alloy was studied in detail in [20]. However, in the professional literature, there is not enough information about the nature of microstructural evolution in plastic deformation processes. The purpose of this work is to study the evolution of the microstructure of the AA2030 alloy in implementing SPD using the method of equal-channel

*Corresponding author: e-mail address: Vi-ta.z@mail.ru

Table 1. The stoichiometric composition of the inclusions in the annealed and ECAP alloy

Symbol	Stoichiometric composition	Phase
Al	$Al_{72.61-81.22}Fe_{6.62-9.98}Cu_{3.88-7.81}Si_{4.63-6.85}Mn_{2.67-4.5}$	$(Fe,Mn)_xSi(Al,Cu)_y$
θ	$Al_{68.87-75.28}Cu_{25.18-31.13}$	Al_2Cu
Pb	$Al_{18.9-67.13}Pb_{18.52-44.33}O_{8.54-37.04}Cu_{1.41-5.13}$	$Al_{13}Pb_{10}O_7Cu$

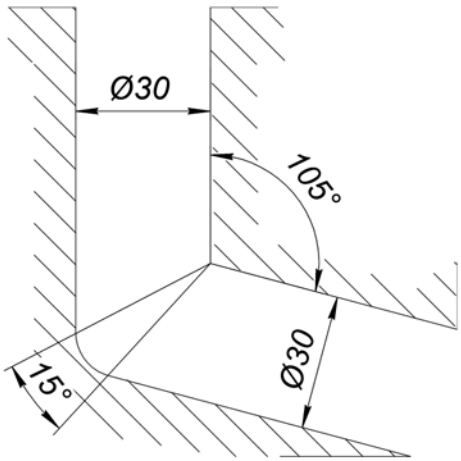

Fig. 1. A tool for implementing the ECAP.

angular pressing (ECAP) and subsequent long-term aging.

2. Material and methods of study

An extruded AA2030 alloy (Al-3.89Cu-1.25Pb--0.8Mg-0.55Mn-0.31Fe-0.2Si, wt.%) in the form of bars with a diameter of 30 mm was used for the study. The workpieces were cut to length of 100 mm each. Before the ECAP, the blanks were treated by annealing at 480 ℃ in a chamber electric furnace. Next, the samples were pressed on the B_c and C routes in a 105°-tool with a plunger speed of 5 mm s^{-1} at the room temperature. The tool had an external rounding angle of 15° (Fig. 1). Then all the samples were subjected to long-term natural aging at room temperature within 45 months.

There were cut transverse and longitudinal samples from each sample to evaluate inclusions on a scanning electron microscope (SEM) and in the transverse direction 3 mm discs for examination on a transmission electron microscope (TEM). A JSM 6490LV electron microscope illustrated their micrography and phase composition. The fine structure was studied on a JEM 2100 transmission electron microscope. For elemental microanalysis of the studied phases, an energy dispersive spectroscopy device (EDS analysis) was used in the SEM and TEM studies.

3. Results and their discussion

3.1. Evolution of inclusions

After annealing, the alloy contains a large number of big constituents located along the axis of primary extrusion (Fig. 2). Using the EDS analysis (Fig. 3), the SEM constituents were identified as Al_2Cu phases designated as θ, the phase $(Fe, Mn)_xSi(Al, Cu)_y$ is designated as (Al), and the complex oxide $Al_{13}Pb_{10}O_7Cu$ is designated as (Pb) (Table 1). In the main matrix, there are fixed dissolved elements such as Mg, Mn, and Cu. Lead particles in the alloy are detected only in combination with oxygen, aluminum, and copper; thus, all of the lead is bound into a complex oxide. In the process of the ECAP treatment there takes place crushing of constituents, turning relative to the original location, partial dissolution. Large constituents on the longitudinal sections have a line structure with a length of up to 50 μm and up to 10 μm in the transverse direction each; on the transverse sections, the particles have an irregular shape with sizes up to 15 μm. The position of small inclusions (smaller than 1 μm) coincides with the outlines of grain boundaries (Fig. 4).

The transformation of small inclusions in the ECAP process was detected using SEM microscopy. When carrying out the 1st cycle of deformation of inclusion of a bar-shaped, sometimes elliptical form, they are mainly located along the grain boundaries. The particles are so dense that they form continuous precipitates. The size of the inclusions ranges from 500 to 1000 nm in length and up to 100 nm in width. The particles were probably separated in the annealing process along the grain boundaries in the form of a continuous mesh. Implementation of the first cycle led to fragmentation (the arrows indicate the location of the inclusions destruction) of the continuous mesh and the formation of bar-shaped particles. The deformation route determines the subsequent behavior of the inclusions. So, after 3 cycles of the ECAP along the B_c route, the described characteristics of the location of the particles is observed, and even after the 4th cycle, fragments of the location of particles along

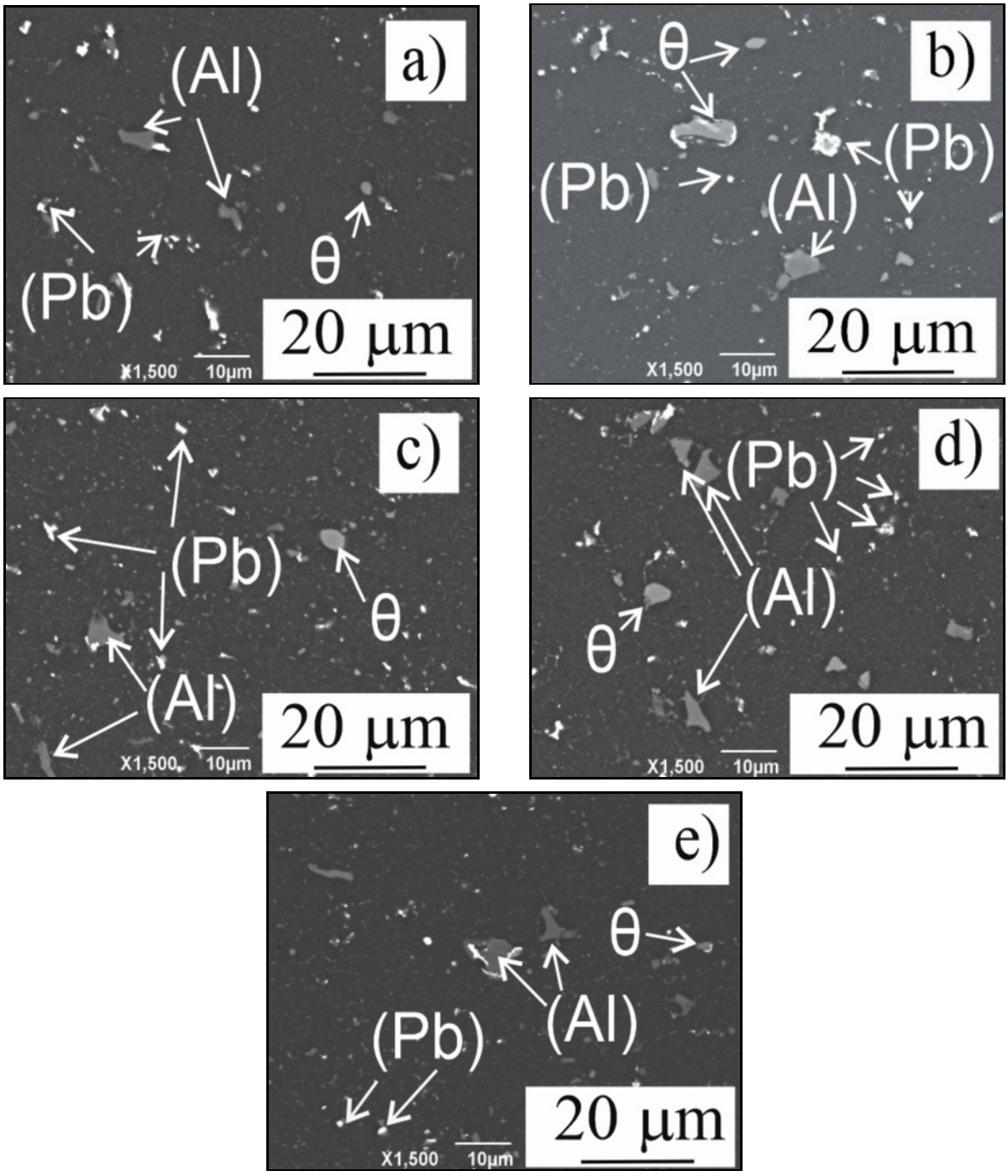

Fig. 2. Constituents in the ECAP treated AA2030 alloys after the 1st cycle of deforming (a), (b), (c) after the 3rd cycle, (d), (e) after the 4th cycle; (b) and (d) the B_c route, (c) and (e) the C route, × 1500.

the grain boundaries are revealed. On the other hand, the C route contributes to the chaotic arrangement of particles after the 3rd and 4th cycles of deformation. It is noticeable that increasing the accumulated degree of deformation during the ECAP narrowing and even blurring of individual particles occurs. The particle identification by SEM is impossible since their size is too small. It should be noted that a smaller number of bar-shaped particles are detected in samples after aging; this allows concluding that there is significant diffusion in the ECAP-treated and aged samples. Figure 5 shows the map of the elements distribution obtained using the EDS of the TEM analyzer. The difference from the coarse-grained analogs is the smearing of detected inclusions, concluding that diffusion is enhanced in the UFG materials obtained by the SPD methods. Intermetallic inclusions detected by TEM in naturally aged samples are represented by four main

Table 2. The stoichiometric composition of inclusions in ECAP and aged alloy

Symbol	Shape	Stoichiometric composition	Phase
Al_7Cu_3Fe	Rod-shape	$Al_{81.88-88.47}Cu_{11.44-11.88}Mn_{0.09-0.15}Fe_{0.01-0.09}$	Al_7Cu_3Fe
θ	Plate-shape	$Al_{71.31-84.85}Cu_{14.08-28.57}Mn_{0.08-1.07}$	Al_2Cu
Pb	Cloud-shape	$Al_{75.41-83.09}Cu_{6.94-17.69}O_{5.72-9.37}Pb_{0.45-1.19}$	Pb-rich complex oxide
Dispersoid	Dispersoid	$Al_{86.34-88.71}Cu_{5.65-7.15}Mn_{5.38-5.98}Fe_{0.27-0.52}$	$Al_{20}Cu_2Mn_3$

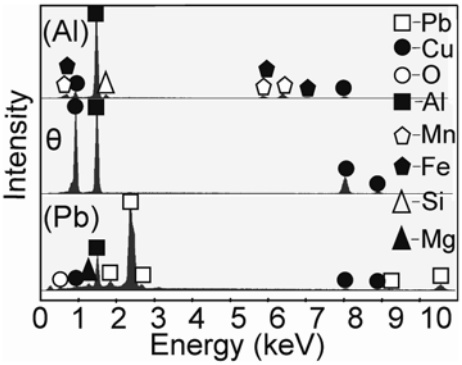

Fig. 3. EDS analysis of constituents shown in Fig. 2.

types: dispersoids, particles of a bar-shaped form, inclusions of a lamellar form, and oxide inclusions rich in lead. In addition, there are particles of silicon with a strong diffraction contrast. The stoichiometric composition of the inclusions after aging is shown in Table 2.

The authors of work [21] note the restriction of UFG materials obtained with a small number of deformation cycles due to the uncontrolled release of inclusions along the grain boundaries during natural aging. The authors found a random orientation of the θ-Al_2Cu phase and its direct formation bypassing the intermediate non-equilibrium phases θ' and θ'', typical for coarse-grained materials. On the other hand [22], the presence of both non-equilibrium phases and the Guinier-Preston zones in the ECAP of Al-Cu treated alloys is noted. J. Gubicza et al. [23] noted that the ECAP affects not only the kinetics of forming inclusions but also their shape for the η phase in the Al-Zn-Mg alloy, which was found only in spherical shape but not in needle-shaped. Similarly, after the ECAP there were detected only spherical flat precipitates of θ-phases with an average size of 500 nm or smaller. At the same time, complete dissolution was noted in [24] after 8 cycles of the ECAP and further separation along the grain boundaries. At this, in [25], bimodality of the observed inclusions is noted. It should be noted that the authors of [26] found that the deformed θ'-particle in the Al-Cu binary alloy dissolves faster than the non-deformable θ-particle due to the additional increasing deformation energy accumulated in the deformed θ-plate, as well as the fragmentation of the particle with the ECAP. Huang Liu et al. [27] also stated the complete dissolution of θ'-particles in Al-Cu binary alloys treated with SPD. It was noted [28] that grinding the grains in ultrafine-grained materials affects the dislocation substructure, which, in turn, regulates the kinetics of inclusions.

In the annealed samples, we recorded the Al_5Cu_2 phase, whose stoichiometric composition differs from the θ-phase by a large amount of aluminum. Moreover, this difference is amplified in the samples after natural aging; incoherent inclusions with the $Al_{2-4}Cu$ composition were detected. For all ECAP modes in naturally aged samples, a significantly larger quantitative run-up of atomic composition than 2 : 1 was detected. After natural aging, the transformation of the θ-phase into the $Al_{2.5-6}Cu$ phase is detected. This indicates the dissolution of the initial particles of the θ-phase after the ECAP during subsequent natural aging. In all the θ-particles, there is an insignificant (less than 1 %) amount of manganese. Probably, manganese replaces part of the copper atoms in the compound. In all the cases, we found a lamellar form of the θ-phase after the ECAP; probably, these inclusions were formed during annealing, and later on, with the ECAP and aging, their slow dissolution occurred. Interestingly, the dissolution of the particles of the θ-phase can occur in two ways. In the first case, which is a priority, there is gradual blurring of the particle accompanied by decreasing the diffraction contrast until it is completely dissolved. There are also several cases when the dissolution of the particle occurs from the periphery to the center of inclusion. In this case, the central layers retain a bright diffraction contrast, and the particle acquires an elliptical shape with strongly elongated long axes. At the same time, its stoichiometric composition does not differ from that described above.

The dispersoids (the $Al_{20}Cu_2Mn_3$ phase) with a size smaller than 100 nm have a fairly constant composition and are located mainly along the grain boundaries. Bar-shaped particles have similar composition but contain additionally iron atoms. Based on the assumptions [29, 30], it is possible to indicate them as particles of the Al_7Cu_3Fe phase.

The dispersoids and Fe-enriched particles effectively interact with structural dislocations. Interestingly, the Al_7Cu_3Fe-phase particles in UFG materials

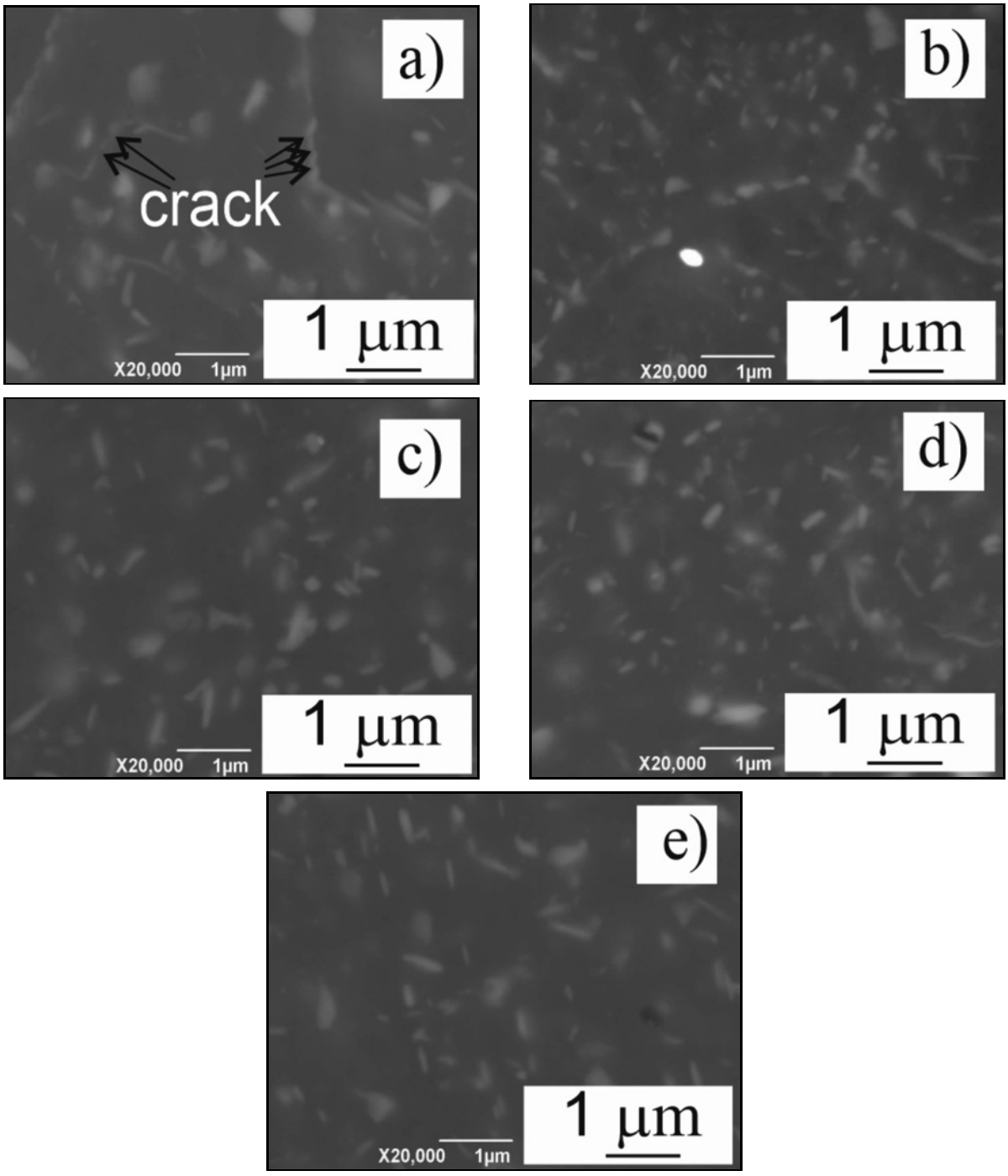

Fig. 4. Evolution of bar-shaped inclusions in the ECAP treated AA2030 alloys after the 1st deformation cycle (a), (b), (c) after the 3rd cycle, (d), (e) after the 4th cycle; (b) and (d) B_c route, (c) and (e) C route, × 20000.

obtained via the B_c route have a large phase contrast compared to the C route, which indicates their lower solubility. A characteristic feature of Al_7Cu_3Fe inclusions is their location either along the grain boundary or across it. Thus, Al_7Cu_3Fe and the dispersoids provide pinning of grain boundaries, restraining their migration and contributing to the grinding of the latter. In addition, these particles and θ-phase particles act as nuclei during grain formation.

An interesting fact is that Pb-rich particles are not involved in the formation of the deformation structure. Lead-containing complex oxides do not interact with dislocations or with other inclusions. Oxides are located both inside the grains and in adjacent grains, while the grain boundaries do not undergo any changes. Thus, the presence of lead does not predict a negative effect on the deformation behavior of the alloy or its mechanical characteristics.

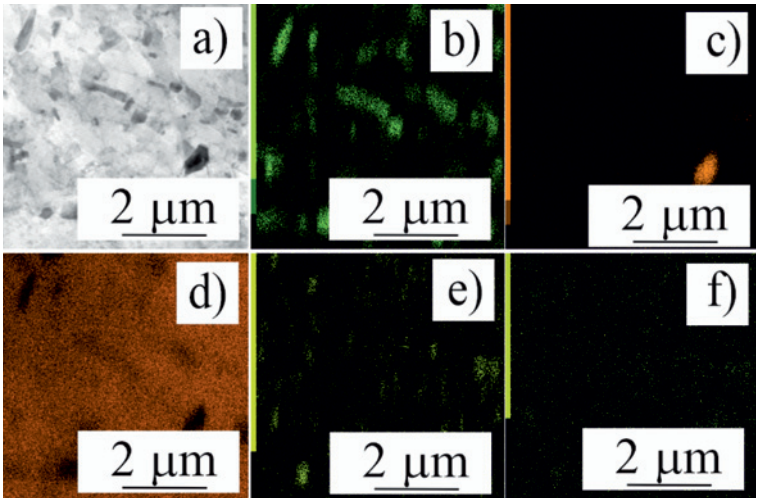

Fig. 5. The map of elements distribution in the ECAP treated AA2030 alloy after long-term natural aging: (a) general, (b) Cu, (c) Si, (d) Al, (e) Mn, and (f) Fe.

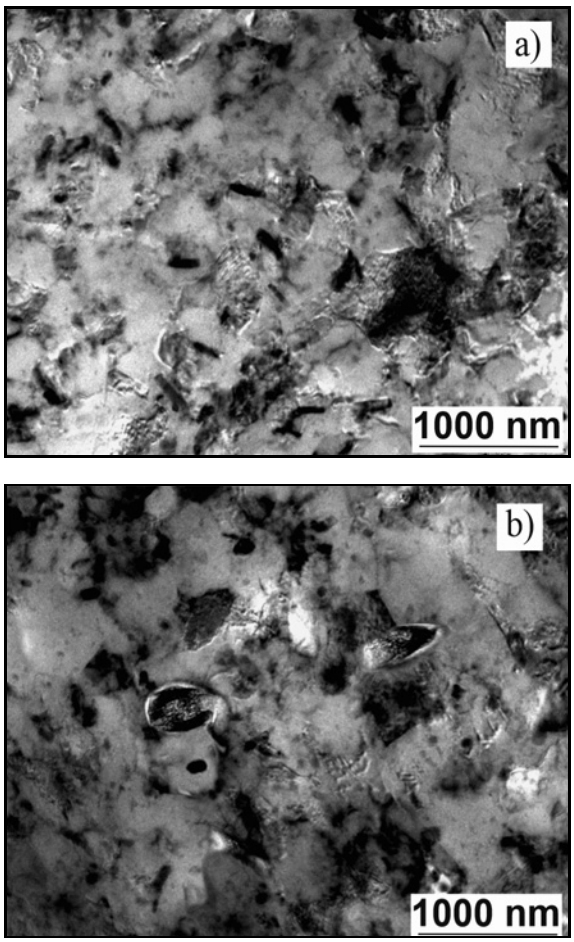

Fig. 6. Microstructure of the ECAP treated AA2030 alloy: (a) B_c route and (b) C route.

3.2. Deformation structures

After the annealing treatment, the grain size observed using optical microscopy was 4 ± 1.5 μm. There was a uniform distribution of grain throughout the cross-section of the workpiece without abnormal grain sizes. The average grain size of the ECAP-treated samples is 420 and 380 nm along the B_c and C routes, respectively (Fig. 6). The structures formed in the UFG AA2030 alloy are distinguished by the coexistence of grains saturated with and free from dislocations. As the degree of deformation increases, the dislocation density in the grains increases, leading to the formation of dislocation tangles and dislocation cells. An intense diffraction contrast in grains with high dislocation density indicates significant stresses. With increasing the growth of the total strain, deformation bands and dislocation walls are formed that may be accompanied by rotation of separate fragments of grains relative to each other.

The deformation structures in the samples after long-term natural aging are of great interest. The coexistence of differently oriented grains/subgrains of different sizes in one grain is typical for ultra-fine-grained structures obtained by SPD. Figure 7a shows many subgrains with low-angle borders formed inside one large grain. It should be noted that the boundary between the G1 and G2 subgrains is not completely formed and is represented by a network of grain-boundary dislocations. The results obtained are in good agreement with the materials presented in [31]. The presence of non-equilibrium boundaries is typical for structures obtained due to realizing large deformations. Figure 7c shows an example of such non-equilibrium structures observed in aged samples. At the same time, a large number of grains with the size of 300–400 nm were found, having a bright diffraction contrast with a cellular structure but free from sub-borders. An electron diffraction pattern typical of single crystals indicates the absence of sub boundaries.

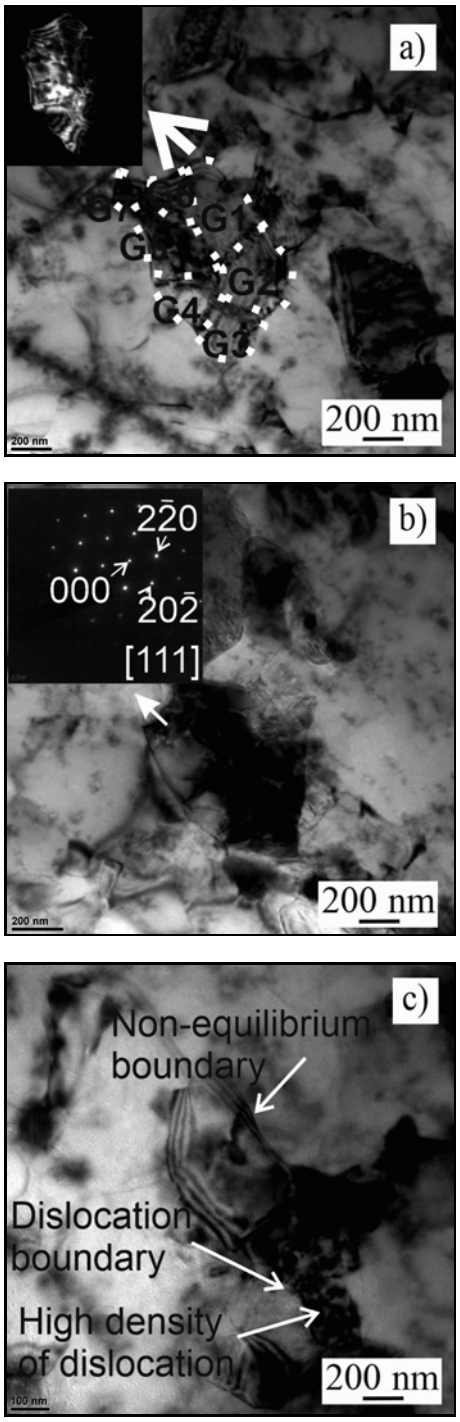

Fig. 7. TEM images of typical grain structures observed in ECAP end aged AA2030 alloys: (a) large grain with subgrains together with dark-field image, (b) grain with dislocation cell structures together with SAD pattern, and (c) typical deformation structure: grain with non-equilibrium boundaries, high density of dislocations.

An interesting fact is the almost complete absence of dislocations in the subgrains.

Thus, the cleaning of grains from dislocations is facilitated by the alignment of dislocations into dislocation walls with the further formation of subgrains and then the grain boundaries. In this case, an important role is played by inclusions that fix dislocations and grain boundaries, thereby acting as embryos in the grain formation. The pattern of forming the described deformation structure is presented in Fig. 8.

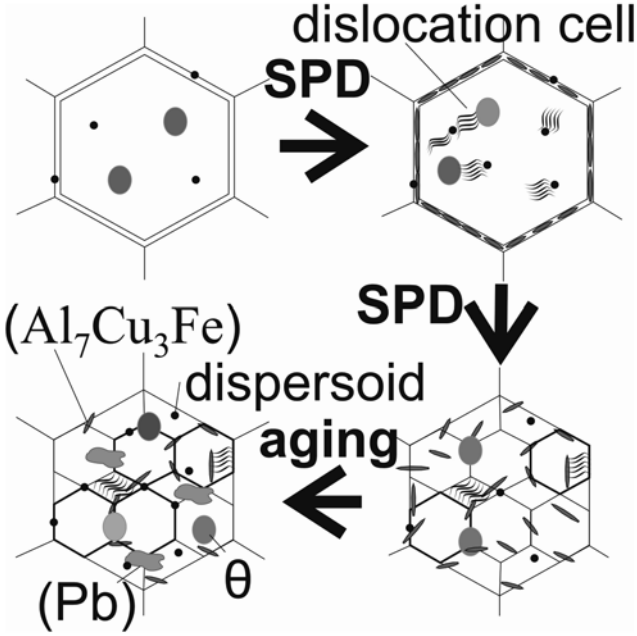

Fig. 8. The pattern of forming the deformation structure in the ECAP treated and aged AA2030 alloy.

4. Conclusions

1. The effect of the ECAP and subsequent long-term natural aging on the evolution of the microstructure of the AA2030 alloy has been experimentally studied. After the ECAP, the alloy has 420 and 380 nm grain sizes obtained by the B_c and C routes, respectively.

2. The ECAP and natural aging after the ECAP lead to the formation of insoluble dispersoids of the $Al_{20}Cu_2Mn_3$ phase providing the pinning of dislocations and grain boundaries.

3. The C route in the ECAP causes more intense dissolution of the particles of the θ-phase and the Al_7Cu_3Fe phase compared to the B_c route.

4. Lead is present in the structure of the AA2030 alloy exclusively in the form of complex oxide and does not take a visible part in the grinding of grains during the ECAP and during subsequent natural aging.

5. In the ECAP-treated samples, spherical θ-phase particles are formed, followed by gradual dissolution in the process of aging. In one case, there takes place

complete dissolution of the particles; in other cases, there is observed the formation of ellipsoidal particles with preserving the $Al_{2.5-6}Cu$ composition.

6. The role of the evolution of inclusions and dislocation cells in the formation of subgrain/grain boundaries has been analyzed, and the mechanisms of grain refinement associated with these structural phenomena have been proposed.

Acknowledgement

The author is grateful to the head of the Department of Materials Science at VSB Technical University of Ostrava, prof. Vlastimil Vodárek, for his assistance in conducting the EDS analysis.

References

[1] Y. Huang, T. G. Langdon, Advances in ultrafine-grained materials, Materials Today 16 (2013) 85–93. https://doi.org/10.1016/j.mattod.2013.03.004

[2] E. Yakushina, A. Reshetov, I. Semenova, V. Polyakova, A. Rosochowski, R. Valiev, The influence of the microstructure morphology of two phase Ti-6Al-4V alloy on the mechanical properties of diffusion bonded joints, Materials Science and Engineering A 726 (2018) 251–258. https://doi.org/10.1016/j.msea.2018.04.052

[3] M. J. Qarni, G. Sivaswamy, A. Rosochowski, S. Boczkal, Effect of incremental equal channel angular pressing (I-ECAP) on the microstructural characteristics and mechanical behaviour of commercially pure titanium, Materials & Design 122 (2017) 385–402. https://doi.org/10.1016/j.matdes.2017.03.015

[4] M. Y. Alawadhi, S. Sabbaghianrad, Y. Huang, T. G. Langdon, Direct influence of recovery behaviour on mechanical properties in oxygen-free copper processed using different SPD techniques: HPT and ECAP, Journal of Materials Research and Technology 6 (2017) 369–377. https://doi.org/10.1016/j.jmrt.2017.05.005

[5] T. Sakai, A. Belyakov, R. Kaibyshev, H. Miura, J. J. Jonas, Dynamic and post-dynamic recrystallization under hot, cold and severe plastic deformation conditions, Progress in Materials Science 60 (2014) 130–207. https://doi.org/10.1016/j.pmatsci.2013.09.002

[6] V. A. Andreyachshenko, A. B. Naizabekov, Microstructural and mechanical characteristics of AlSi MnFe alloy processed by equal channel angular pressing, Metalurgija 55 (2016) 353–356.

[7] A. B. Naizabekov, V. A. Andreyachshenko, Evaluation of possible mechanical property improvement for alloy of the A-Fe-Si-Mn System by Equal-Channel Angular Pressing, Metallurgist 57 (2013) 159–163 https://doi.org/10.1007/s11015-013-9706-0

[8] V. Andreyachshenko, A. Naizabekov, The technology of equal channel angle backpressure extrusion for deformation iron and aluminium alloys, Proceedings of the 3rd International Conference on NANOCON (2011), pp. 246–252.

[9] A. Naizabekov, V.Andreyachshenko, J. Kliber, Forming of microstructure of the Al-Si-Fe-Mn system alloy by equal channel angular pressing with backpressure, Proceedings of the 21st International Conference on Metallurgy and Materials, Metal (2012), pp. 391–395.

[10] V. Andreyachshenko, Evolution of Al-Si-Mn-Fe aluminum alloy microstructure in the equal-channel angular pressing with back pressure, Materials Letters 254 (2019) 433–435. https://doi.org/10.1016/j.matlet.2019.07.127

[11] K. Zheng, D. J. Politis, L. Wang, J. Lin, A review on forming techniques for manufacturing lightweight complex-shaped aluminium panel components, International Journal of Lightweight Materials and Manufacture 1 (2018) 55–80. https://doi.org/10.1016/j.ijlmm.2018.03.006

[12] H. Wang, Y. Huang, W. Zhang, The study of laser shock peening with side-water spraying and coaxial-water feeding technology, International Journal of Lightweight Materials and Manufacture 1 (2018) 102–107. https://doi.org/10.1016/j.ijlmm.2018.05.00

[13] S. Wisutmethangoon, S. Pannaray, T. Plookphol, J. Wannasin, Effect of aging condition on semisolid cast 2024 aluminum alloy, International Journal of Chemical, Molecular, Nuclear, Materials and Metallurgical Engineering 8 (2014) 294–297. https://zenodo.org/record/1091950

[14] A. Smolej, M. Soković, J. Kopač, V. Dragojević, Influence of heat treatment on the properties of the free-cutting AlMgSiPb alloy, Journal of Materials Processing Technology 53 (1995) 373–384. https://doi.org/10.1016/0924-0136(95)01994-P

[15] J. Kopač, M. Soković, A. Smolej, A. Gorcenko, V. Dragojević, Strategy of machinability of aluminium alloys for free cutting, Proceedings of the Thirtieth International MATADOR Conference (1993), London, pp. 151–156. ISBN 978-1-349-13255-3 https://doi.org/10.1007/978-1-349-13255-3_20

[16] G. C. Pratt, W. J. Whitney, U.S. Patent No. 5,053,286. Washington, DC: U.S. Patent and Trademark Office, 1991.

[17] M. F. Miller, F. J. Webbare, U.S. Patent No. 3,545,943. Washington, DC: U.S. Patent and Trademark Office, 1970.

[18] J. Lohse, K. Sander, M. Wirts, Heavy Metals in Vehicles II. Okopol, Hamburg, 2001.

[19] Y. Zedan, A. M. Samuel, F. H. Samuel, H. W. Doty, Effects of Sn, Bi, and Pb addition on the mechanical properties and machinability of Al-11% casting alloys, AFS Proceeding, 11-071 (2011), pp. 3–16.

[20] S. Koch, M. D. Abad, S. Renhart, H. Antrekowitsch, P. Hosemann, A high temperature nanoindentation study of A-Cu wrought alloy, Materials Science and Engineering A 644 (2015) 218–224. https://doi.org/10.1016/j.msea.2015.07.066

[21] L. Jiang, J. K. Li, P. M. Cheng, G. Liu, R. H. Wang, B. A. Chen, G. Yang, Microalloying ultrafine grained Al alloys with enhanced ductility, Scientific Reports 4 (2014) 3605. https://doi.org/10.1038/srep03605

[22] M. Cabibbo, Adiabatic heating and role of the intermetallic phase on the ECAP-induced strengthening in an Al-Cu alloy, La Metallurgia Italiana 6 (2015) 3–9.

[23] J. Gubicza, I. Schiller, N. Q. Chinh, J. Illy, Z. Horita,

T. G. Langdon, The effect of severe plastic deformation on precipitation in supersaturated Al-Zn-Mg alloys, Materials Science and Engineering: A 460 (2007) 77–85. https://doi.org/10.1016/j.msea.2007.01.001

[24] M. Murayama, Z. Horita, K. Hono, Microstructure of two-phase Al-1.7at.%Cu alloy deformed by equal-channel angular pressing, Acta Materialia 49 (2001) 21–29. https://doi.org/10.1016/S1359-6454(00)00308-6

[25] A. Deschamps, F. De Geuser, Z. Horita, S. Lee, G. Renou, Precipitation kinetics in a severely plastically deformed 7075 aluminium alloy, Acta Materialia 66 (2014) 105–117. https://doi.org/10.1016/j.actamat.2013.11.071

[26] Z. Liu, S. Bai, X. Zhou, Y. Gu, On strain-induced dissolution of θ' and θ particles in Al-Cu binary alloy during equal channel angular pressing, Materials Science and Engineering A 528 (2011) 2217–2222. https://doi.org/10.1016/j.msea.2010.12.060

[27] W. Huang, Z. Liu, L. Xia, P. Xia, S. Zeng, Severe plastic deformation-induced dissolution of θ'' particles in Al-Cu binary alloy and subsequent nature aging behavior, Materials Science and Engineering A 556 (2012) 801–806. https://doi.org/10.1016/j.msea.2012.07.070

[28] T. Hu, K. Ma, T. D. Topping, J. M. Schoenung, E. J. Lavernia, Precipitation phenomena in an ultrafine-grained Al alloy, Acta Materialia 61 (2013) 2163–2178. https://doi.org/10.1016/j.actamat.2012.12.037

[29] J. E. Hatch, Aluminum: Properties and Physical Metallurgy, ASM International, Metals Park, Ohio, 1984, p. 209.

[30] A. E. Hughes, N. Birbilis, J. M. Mol, S. J. Garcia, X. Zhou, G. E. Thompson, High strength Al-alloys: microstructure, corrosion and principles of protection. In: Recent Trends in Processing and Degradation of Aluminum Alloys, Rijeka, Croatia, 2011, pp. 262–516.

[31] M. P. Liu, T. H. Jiang, X. F. Xie, L. Qiang, X. F. Li, H. J. Roven, Microstructure evolution and dislocation configurations in nanostructured Al-Mg alloys processed by high pressure torsion, Transactions of Nonferrous Metals Society of China 24 (2014) 3848–3857. https://doi.org/10.1016/S1003-6326(14)63542-1